Biosensors and Bioelectronics 102 (2018) 403–410

Contents lists available at ScienceDirect

Biosensors and Bioelectronics

journal homepage: www.elsevier.com/locate/bios

PdPt nanoparticles anchored on the N-G with the integration of PANI nanohybrids as novel redox probe and catalyst for the detection of rs1801177

Jing Wu[1], Junlin He[1], Chengli Zhang, Jun Chen, Yazhen Niu, Qiqi Yuan, Chao Yu*

College of Pharmacy, School of Public Health and Management, and Chongqing Pharmacodynamic Evaluation Engineering Technology Research Centre, Chongqing Medical University, Chongqing 400016, PR China

ARTICLE INFO

Keywords:
Novel redox nanoprobe
Catalytic signal amplification
Lipoprotein lipase gene
Atherosclerosis
DNA biosensor

ABSTRACT

Single nucleotide polymorphism (SNP) in lipoprotein lipase (LPL) gene (rs1801177) is strongly associated with the increased progression of atherosclerosis, threatening global public health. In this work, a relatively simple, specific and ultrasensitive electrochemical DNA biosensor was constructed to detect rs1801177 for the first time. A glass carbon electrode was modified with fullerene (C_{60})/polyamidoamine (PAMAM)/gold (Au) nanoparticles nanocomposites film. In addition the nitrogen-doped graphene (N-G)/palladium platinum (PdPt) bimetallic nanoparticle/ polyaniline (PANI) nanohybrids were synthesised and used to label the signal probes. These nanohybrids have abundant active groups, and efficient redox and catalytic activity, allowing them to be used as the nanocarrier for a redox nanoprobe without the additional modification of electroactive substance and catalyst, which could effectively simplify the operation procedure and shorten the analysis time. With the catalysis of H_2O_2 by nanohybrids, the detection signal of N-G/PdPt/PANI itself could be significantly enhanced, lead to the improvement of the sensitivity. Under optimal conditions, the electrochemical DNA biosensor exhibited desirable performance for the determination of rs1801177 with a wide linearity ranging from 10 fM to 10 nM and a relatively low detection limit of 3.33 fM (S/N = 3). The proposed biosensor showed excellent selectivity to the target DNA compared to possible interfering substances. The results suggested that this method has potential applications in clinical research.

1. Introduction

Cardiovascular disease (CVD) is caused by atherosclerosis and has become a major cause of global morbidity and mortality (Ding et al., 2017; Tapiavieyra et al., 2017). The missense single nucleotide polymorphism (SNP) (rs1801177, G280A, Asp9Asn, D9N) in the coding region of the lipoprotein lipase (LPL) gene is strongly associated with the increased progression of atherosclerosis (Jukema et al., 1996). The LPL gene SNP rs1801177 can be used to predict cardiovascular disease risk directly. Thus, the SNP of LPL gene would become a biomarker for clinical research and diagnosis (Rebhi et al., 2012). With this consideration, the determination of rs1801177 in LPL gene is of great importance for the early diagnosis, treatment and prognosis evaluation.

Various techniques for the detection of rs1801177 (D9N) in LPL gene have been reported, such as DNA sequencing (Shahid et al., 2017), polymerase chain reaction restriction fragment length polymorphism (PCR-RFLP) (Izar et al., 2009) and TaqMan assays (Junyent et al., 2010). However, DNA sequencing has the disadvantages of relatively expensive and insensitive (C.Z. Wang et al., 2013). PCR-RFLP consists of several steps including an electrophoretic separation step, which is relatively complicated and time-consuming (Zhang et al., 2005). For TaqMan assays, the major disadvantage is the requirement of expensive fluorescence-labelled probes (Pichler et al., 2009). Thus, these shortcomings considerably hindered the application of these approaches in the clinical setting. Compared with these methods, electrochemical DNA biosensors have drawn considerable attention owing to the advantages including simplicity, rapidity and cost-effectiveness (Ruiyi et al., 2016). Furthermore, electrochemical DNA sensors are highly specific and sensitive without requiring sophisticated instruments (Yao et al., 2013). Therefore, there is an urgent need to find a DNA-based electrochemical biosensor with high sensitivity and selectivity for SNP genotyping appears. To our knowledge, the electrochemical detection of the rs1801177 of LPL gene has not yet been reported. To develop an electrochemical DNA biosensor for the detection of rs4839469 in LPL

* Correspondence to: College of Pharmacy, Chongqing Medical University, 1 Yi Xue Yuan Road, Box 380#, Chongqing 400016, PR China.
E-mail address: yuchaom@163.com (C. Yu).
[1] Junlin He and Jing Wu contributed equally to this work.

https://doi.org/10.1016/j.bios.2017.11.054
Received 18 August 2017; Received in revised form 11 November 2017; Accepted 17 November 2017
Available online 21 November 2017
0956-5663/

gene is not only important but also necessary.

Fullerene (C_{60}), a zero-dimensional carbon, of significant interest to researchers, showed promising application prospects in biosensor when it was first discovered by Kroto owning to its unique physical and chemical properties such as large specific surface area (Zhong et al., 2012), strong electron-accepting capacity and excellent electrochemical conductivity (Afreen et al., 2015). But the aggregation and unstability of C_{60} in water hinders its application (Prasad et al., 2017). Upon consideration of these problems, Sivakumar and his co-workers have synthetized the potential fullerenol moieties [$C_{60}(OH)_n{\cdot}mH_2O$] to improve the defects (Afreen et al., 2017). However, in our work, the polyamidoamine (PAMAM) dendrimers was chosen to solve this problem. Because the PAMAM dendrimer is a type of hyper-branched, tree-like molecule with a large number of amino groups that can effectively prevent C_{60} from aggregation as well as load many gold (Au) nanoparticles to combine a large number of capture probes (CPs) and enhance the sensitivity of the electrochemical DNA biosensor (Astruc et al., 2010; Huang et al., 2015; Liu et al., 2014).

To achieve signal amplification and superior sensitivity of the electrochemical DNA biosensor, nitrogen-doped graphene (N-G)/palladium platinum (PdPt) bimetallic nanoparticles/polyaniline(PANI) nanomaterials were synthesised and used to label signal probes (SPs) for the first time. Graphene, a single-atom-thick sheet of hexagonally arrayed sp^2-bonded carbon atoms (R.G. Bai et al., 2017), has been shown to have many promising applications in eletrochemical biosensors with excellent mechanical stability and electrical conductivity (Geetha et al., 2017; Zan et al., 2013). Compared with graphene, N-G has drawn more attentions due to the introduction of nitrogen. The N-G has much a higher ratio in surface-active groups can increased biocompatibility of the C/N microenvironment (Yang et al., 2013); it also has better electrical conductivity for the acceleration of electrons (Chen et al., 2016) and more chemical active sites for the further functionalization with metal nanoparticles (Jiang et al., 2014). Furthermore, N-G with nitrogen atoms doping can serve as an excellent platform for loading metal nanoparticles and introducing defective sites on the graphene surface to improve the electrocatalytic activities of metal nanoparticles for the amplification of electrochemical signal and thus increase the sensitivity of DNA biosensor (Thanh et al., 2016).

To further improve the sensitivity of the DNA biosensor, PdPt bimetallic nanoparticles were used to anchor on the N-G sheet. Pd and Pt nanoparticles hold excellent biocompatibility for biomolecules and good catalytic activity (M. Li et al., 2017). In addition, with the participation of two metals, the PdPt bimetallic nanoparticles have stronger catalytic activity to H_2O_2 than the single metal, owning to the synergistic effect of bimetals (Ghadimi et al., 2015; Y. Li et al., 2017b). Although, the N-G anchored by PdPt bimetallic nanomaterials does contribute to the amplification and enhancement of the sensitivity in the electrical signal, the DNA molecule cannot act as a redox probe intrinsically. Therefore, it is often necessary to consider the introduction of a redox probe which determines the detection limit, linear range and sensitivity in the construction of the DNA biosensor. The use of nanomaterial itself as the redox probe (such as Prussian blue or metallic hexacyanoferrates) has been widely used with the advantages of enhancing the number of immobilized biomolecules as nanocarriers and avoiding the leakage of redox molecules efficiently (Han et al., 2012; Lai et al., 2009). Polyaniline (PANI) with polymer chain structures can serve as an effective redox mediator for further signal amplification owing to its environmental stability, easy synthesis and high controllable conductivity (Chen et al., 2017; Dhand et al., 2011). Moreover, with the dopant of acid (Liu et al., 2012; Z.G. Wang et al., 2013) or metals (Sivakumar and Gedanken, 2005), the conductivity and thermoelectric property of PANI could be increased by several orders of magnitude.

Herein, a novel sandwich-type electrochemical DNA biosensor with the advantages including simplicity, rapidity, specificity and sensitivity was constructed for the detection of rs1801177 in LPL gene. C_{60}/PAMAM/Au nanomaterials served as a composite film were used to modify the electrode. N-G/PdPt/PANI nanohybrids were used to label the signal probes, which could generate signals by themselves and act as catalyst without the additional modification of electroactive substance and catalyst. Additionally, it can simplify the operation procedure and shorten the analysis time. Moreover, the nanohybrids could be used to catalyze the H_2O_2 reaction, enhancing the electrochemical signal to realise the amplification of the detection signal. Therefore, the sensitivity of the DNA biosensor was increased significantly. To the best of our knowledge, the N-G/PdPt/PANI nanomaterials were prepared and used in a DNA biosensor for the first time in this work. At the same time, this study demonstrates the first electrochemical specific detection of rs1801177 in LPL gene.

2. Experimental

2.1. Reagents and materials

The materials and reagents are described in detail in Supplementary information (S1.1).

2.2. Apparatus and measurements

The apparatus is described in detail in Supplementary information (S1.2)

2.3. Preparation of C_{60}/PAMAM/Au nanomaterials

The details of the preparation of the C60/PAMAM/Au nanomaterials can be found in Supplementary information (S1.3).

2.4. Preparation of N-G/PdPt/PANI, N-G/Pd/PANI and N-G/Pt/PANI nanohybrids

The N-G/PdPt nanocomposites were prepared using a procedure available in literature with a slight modification (Adams et al., 2011). Briefly, 10 mg N-G was added to a solution mixture of 2.6 mL $H_2PtCl_6{\cdot}6H_2O$ (3.5 mM) and 3 mL Na_2PdCl_4 (3 mM), followed stirring with ultrasonication for 1 h. The pH of the solution-mentioned above was then adjusted to a value of 9.5–10 by the addition of NaOH (0.05 mM) and stirred for 10 min. Next, 25 mL $NaBH_4$ (0.01 M) was added dropwise into the solution. After 3 h, the N-G/PdPt nanomaterials solution was centrifuged and washed by ultrapure water to obtain the N-G/PdPt nanocomposites. The resulting N-G/PdPt nanocomposites were redissolved in 10 mL ultrapure water. Next, 10 mL of this N-G/PdPt solution and 100 μL aniline were added to 5 mL H_2SO_4 (0.5 M) under stirring. Subsequently, 5 mL $K_2S_2O_8$ (0.15 M) was added dropwise to the N-G/PdPt nanomaterials solution under continuous stirring for 6 h at 0 °C. After centrifuging and washing, the resulting nanohybrids were redissolved in 10 mL ultrapure water and stored in the refrigerator at 4 °C for further use. The N-G/Pd/PANI and N-G/Pt/PANI nanomaterials were synthesised using the same procedure as that for N-G/PdPt/PANI but without the addition of $H_2PtCl_6{\cdot}6H_2O$ (3.5 mM) or Na_2PdCl_4 (3 mM) respectively. The preparation process of the N-G/PdPt/PANI nanocomposites is displayed in Scheme 1B.

2.5. Preparation of N-G/PdPt/PANI/SP/MCH, N-G/Pd/PANI/SP/MCH and N-G/Pt/PANI/SP/MCH bionanocomposites

In brief, 200 μL carboxylated SP (2 μM), 2 mL N-G/PdPt/PANI solution, 2 mL 1-ethyl-3-(3-dimethylaminopropyl)-carbodiimide hydrochloride (EDC, 400 mM) and 2 mL N-hydroxysulphosuccinimide (NHS, 100 mM) were stirred for 12 h at 4 °C. After the SP was conjugated onto the surface of N-G/PdPt/PANI nanohybrids through the amide reaction, the excess reagent was centrifuged and washed using ultrapure water and redissovled in 2 mL ultrapure water. Subsequently, 200 μL 6-

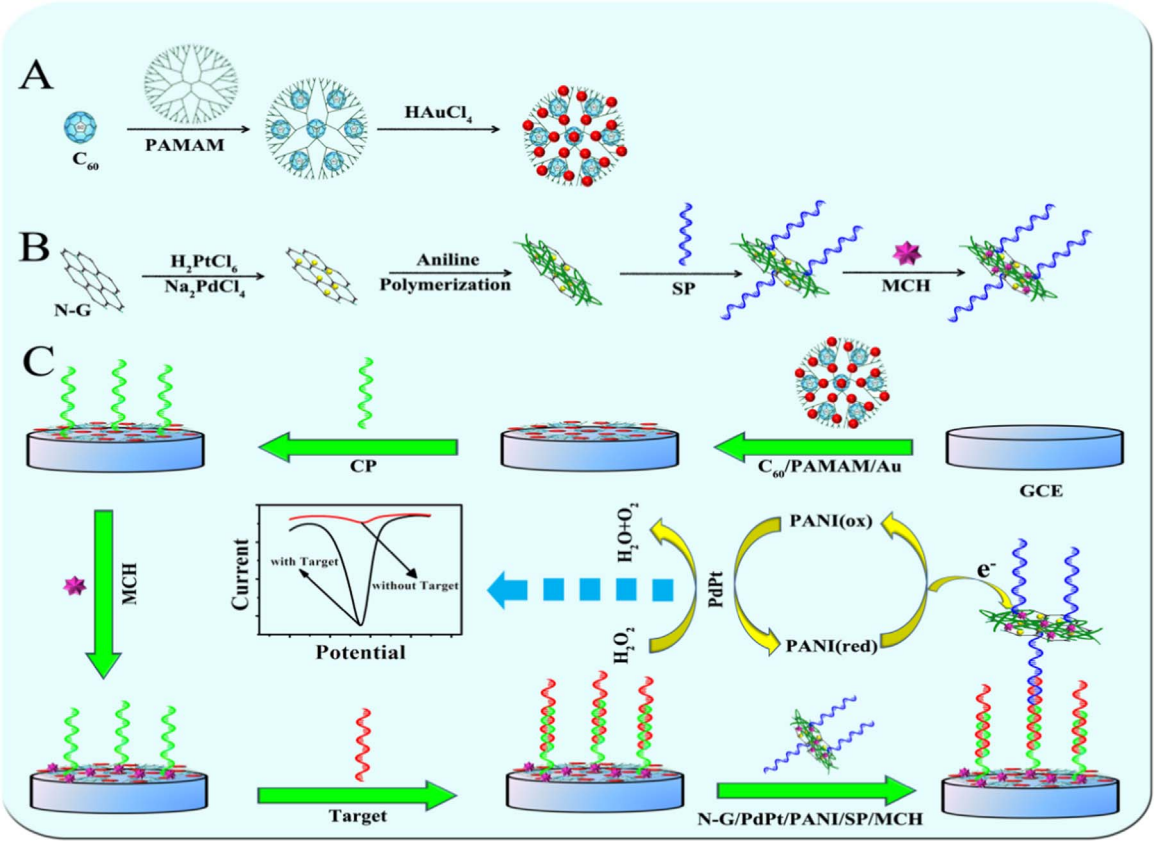

Scheme 1. (A) Scheme of the preparation process of the C_{60}/PAMAM/Au nanocomposites, (B) scheme of the preparation process of the N-G/PdPt/PANI/SP/MCH bioconjugates and (C) scheme of the electrochemical DNA biosensor fabrication.

mercapto-1-hexanol (MCH, 1 mM) solution was added to this mixture and stirred for 4 h to block non-specific binding sites on the surface of the N-G/PdPt/PANI nanohybrids at 4 °C. The excess reagents were removed by centrifugation, and the obtained N-G/PdPt/PANI/SP/MCH bioconjugates were then dispersed in 2 mL ultrapure water and stored at 4 °C before use (these maintained their electrochemical activity for 15 d). The N-G/Pd/PANI/SP/MCH and N-G/Pt/PANI/SP/MCH bioconjugates were synthesised using a similar process as that for N-G/PdPt/PANI/SP/MCH, except that N-G/PdPt/PANI nanohybrids replaced by N-G/Pd/PANI nanomaterials and N-G/Pt/PANI nanocomposites respectively. The preparation process of the N-G/PdPt/PANI/SP/MCH bioconjugates is displayed in Scheme 1 B.

2.6. Fabrication of the DNA biosensor

To obtain a mirror-like surface, a glassy carbon electrode (GCE, with diameter of 4 mm) was polished successively with 0.3 and 0.05 μm alumina slurries, followed by ultrasonic treatment in ethanol and ultrapure water. The GCE was then allowed to dry in air at room temperature (RT). Subsequently, 8 μL C_{60}/PAMAM/Au nanohybrids solution was dropped onto the pretreated GCE surface and dried in air at RT. Afterwards, 20 μL of the 2 μM capture probe was dropped onto the modified GCE surface and incubated for 12 h at 37 °C. The GCE surface was then rinsed with ultrapure water and blocked with 20 μL MCH solution (1 mM) for 1 h at 37 °C. The stepwise process for the construction of the DNA biosensor is displayed in Scheme 1 C. And the interface properties of the surface modified electrodes were investigated by cyclic voltammetry (CV) and electrochemical impedance spectroscopy (EIS) in 5 mM $Fe(CN)_6^{4-/3-}$ solution containing 0.1 M KCl.

2.7. Detection of target DNA

Before measurement, the as-prepared DNA sensor was incubated with 20 μL target DNA solution of various concentrations for 2 h at 37 °C. Subsequently, the prepared DNA biosensor was rinsed and incubated with 10 mL of the tracer label for another 2 h at 37 °C. The obtained biosensors were investigated by differential pulse voltammetry (DPV) in 0.1 M PBS buffer (pH = 7.0) with 2.5 mM H_2O_2. The electrochemical response signal originated from the N-G/PdPt/PANI nanohybrids in tracer label and was further amplified by the electrocatalysis of H_2O_2 through the N-G/PdPt/PANI nanohybrids, which gave rise to the electrochemical detection of rs1801177 in LPL gene.

3. Results and discussion

3.1. Morphology and structural characterisation of the different nanohybrids

The size and morphology of the as-prepared nanohybrids were characterised using field emission scanning electron microscopy (FE-SEM) images. As shown in Fig. 1A, the N-G consists of lamellate and tulle-like structures, in addition to wrinkles and folds, suggesting that the high surface/volume ratio and the two-dimensional structure of the graphene were well maintained. After the reduction of H_2PtCl_6 and Na_2PdCl_4 by $NaBH_4$, a homogeneous and dense coverage of PdPt bimetallic nanoparticles on the surface of N-G can be seen, shown in Fig. 1B, indicating the successful synthesis of N-G/PdPt nanohybrids. After the aniline was polymerized to PANI, abundant filiform tubules are uniformly dispersed on the surface of the N-G/PdPt (Fig. 1C), confirming the formation of N-G/PdPt/PANI nanohybrids. XPS was carried out to further analyse the surface chemical composition and status of the N-G/PdPt/PANI nanohybrids. The characteristic peaks for

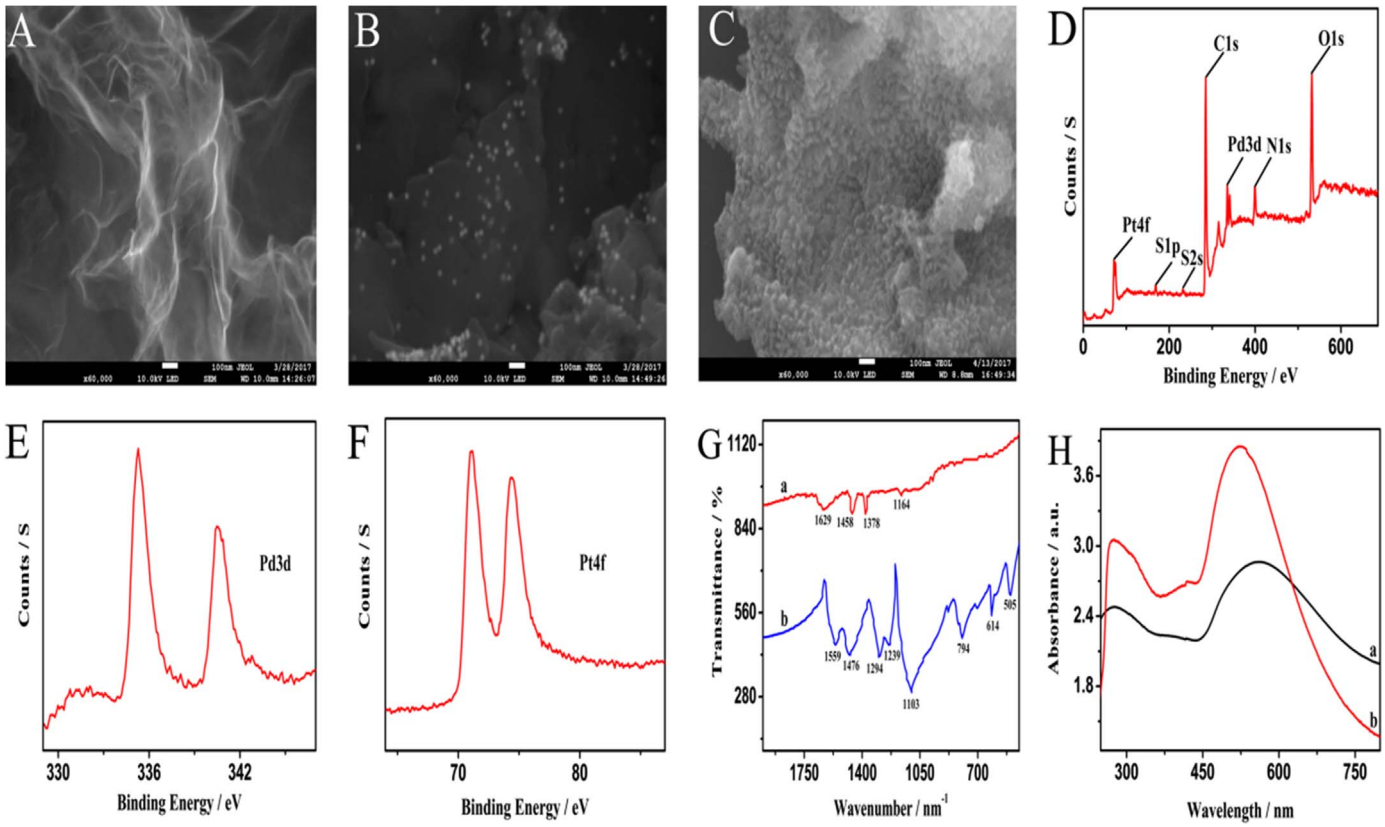

Fig. 1. FE-SEM images of different nanohybrids: (A) N-G sheets, (B) N-G/PdPt nanohybrids and (C) N-G/PdPt/PANI nanohybrids. (D) XPS spectra of N-G/PdPt/PANI nanohybrids. XPS analysis for Pd3d (E) and Pt4f (F) core levels of N-G/PdPt/PANI nanohybrids. (G) FT-IR spectra of N-G (curve a) and N-G/Pdpt/PANI nanohybrids (curve b). (H) UV–Vis absorption spectra of (a) PANI and (b) N-G/PdPt/PANI nanohybrids.

Pt4f, S2p, S2s, C1s, Pd3d, N1s and O1s core-level regions can be clearly observed for the N-G/PdPt/PANI nanohybrids in Fig. 1D. In addition, Pd3d peaks are observed at binding energies of 340.48 eV and 335.28 eV in Fig. 1E and Pt4f peaks can be seen at binding energies of 74.38 eV and 71.08 eV in Fig. 1F, conforming that the bimetallic nanoparticles of PdPt are successfully anchored on the N-G sheets. The structural features of N-G and N-G/PdPt/PANI nanohybrids were characterised using Fourier transform infrared (FTIR) spectroscopy (Fig. 1G). In the FTIR spectra of N-G (curve a), the absorption peak at 1629 cm^{-1} is attributed to the characteristic C=N stretching band (Pu et al., 2017), the absorption band at 1458 cm^{-1} is ascribed to the bending vibration of C-C (Zhang et al., 2017), and the two peaks at 1164 and 1378 cm^{-1} are as a result of C-H bending vibrations (Jian-Min et al., 2017; Zhang et al., 2011). For the N-G/PdPt/PANI nanohybrids (curve b), the characteristic bands at 1559 and 1476 cm^{-1} are related to C=C stretching vibration modes in the quinoid and benzene rings (Zheng et al., 2012), respectively, whereas the bands at 1292 and 1236 cm^{-1} are assigned to C-N stretching of the benzenoid group (Geng et al., 2011). Additionally, the bands at 1102 and 797 cm^{-1} are attributed to the C-H in-plane bending and the C–H out-of-plane bending modes, respectively (Ma et al., 2010; Wang et al., 2002). Moreover, the peaks at 505 and 614 cm^{-1} are ascribed to the SO_3H groups (Xu et al., 2007; Yin et al., 2008), which prove that the successful doping of H_2SO_4 has occurred. At the same time, the ultraviolet-visible (UV–Vis) absorption spectroscopy was used to analyse the PANI and N-G/PdPt/PANI nanohybrids. As shown in Fig. 1H, the PANI (curve a) shows two absorption peaks at 275 and 551 nm. Both peaks are related to the π→π transition of benzenoid and quinoid rings (Chen et al., 2015). After the surface of N-G/PdPt was covered, the N-G/PdPt/PANI nanocomposites (curve b) display a blue-shift by 7 and 15 nm and show maximum at 268 and 536 nm. It is suggested that a strong interaction forms between PANI and N-G/PdPt nanomaterials. Furthermore, the zeta potentials of the nanomaterials were investigated. As shown in Fig. S2D, the zeta potential of N-G was −17.3 mV (curve a). After the PdPt bimetallic nanoparticles were anchored onto the surface of the N-G, the zeta potential became −37.6 mV (curve b). When the N-G/PdPt nanomaterials were integrated with PANI, the zeta potential changed to 9.63 mV (curve c). All the above results suggest that N-G/PdPt/PANI hybrids were successfully synthesised without the destruction of their structures.

3.2. Electrochemical characterisation of the DNA biosensor

The interface properties of the surface modified electrodes were investigated by cyclic voltammetry (CV); the resulting voltammograms are illustrated in Fig. 2A. A couple of defined redox peaks of $Fe(CN)_6^{4-/3-}$ are observed for the bare glass carbon electrode (curve a). The current response increased after the electrode surface was modified with the C_{60}/PAMAM/Au nanomaterials (curve b), which is attributed to the fact that the C_{60}/PAMAM/Au nanomaterials can significantly enhance the effective surface of the electrode to facilitate the electron transfer. When the capture probes were assembled onto the electrode surface (curve c), the current response decreased, suggesting that negatively charged DNA hindered the diffusion of $Fe(CN)_6^{4-/3-}$ toward the electrode surface. Subsequently, the current response decreased further after the non-specific binding sites on the electrode surface were blocked by the non-electroactive MCH (curve d). When the modified electrode was incubated with the target DNA, the current response decreased dramatically (curve e), because the electrostatic repulsion of double stranded DNA severely hindered the electron transfer of the redox probe $Fe(CN)_6^{4-/3-}$.

The semicircle diameter of the electrochemical impedance spectroscopy (EIS) is equal to the electron transfer resistance (Ret) and the high frequency region of the impedance plot shows a semicircle related

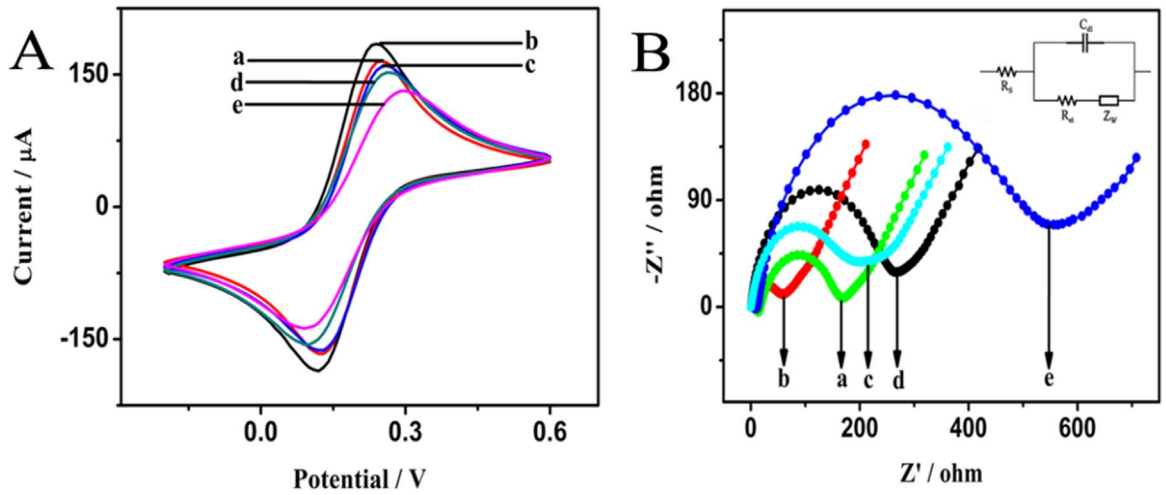

Fig. 2. CV (A) and EIS (B) of different modified electrodes in 5 mM $Fe(CN)_6^{4-/3-}$ solution containing 0.1 M KCl: (a) bare GCE, (b) C_{60}/PAMAM/Au/GCE, (c) CP/C_{60}/PAMAM/Au/GCE, (d) MCH/CP/C_{60}/PAMAM/Au/GCE and (e) Target/ MCH/CP/C_{60}/PAMAM/Au/GCE.

to the redox probe $Fe(CN)_6^{4-/3-}$. Therefore, the stepwise of fabrication process was also monitored using EIS; and the Nyquist diagrams of the redox couple $Fe(CN)_6^{4-/3-}$ at different modified electrodes are displayed in Fig. 2B. It was found that the bare GCE produce a relatively small semicircle (curve a). When the electrode surface was modified by C_{60}/PAMAM/Au nanomaterials, the impedance value decreased (curve b), indicating that the C_{60}/PAMAM/Au nanomaterials were conductive to the transmission of electrons. After the immobilisation of the capture probes, the semicircle diameter increased significantly (curve c), owing to the repulsion between the negative charges on the DNA backbone and $Fe(CN)_6^{4-/3-}$ from the electrode. The resistance increased further when the nonspecific sites on the electrode surface were blocked with the non-conductive MCH (curve d). There was an apparent increase of Ret when the electrode was incubated with the target DNA (curve e), which is attributed to the formation of double stranded DNA obstructing the electron transfer of the redox couple. The fabrication process was also investigated using AFM as shown in Fig. S3, and a detailed description can be found in Supplementary information (S2.2). All the results obtained can be used to further support the successful fabrication and potential applications of the constructed biosensor.

3.3. Comparison of different signal amplification strategies

To evaluate the specific roles of N-G/PdPt/PANI on amplification of detection signal, differential pulse voltammetry (DPV) responses of various nanohybrids-labelled SPs incubated without the target DNA (black curve) served as the background value and with 10 pM target DNA (red curve) were studied in 0.1 M PBS buffer (pH = 7.0) with or without 2.5 mM H_2O_2. As shown in Fig. 3A, the DPV response of the electrochemical DNA biosensor incubated with the target DNA and N-G/PdPt/PANI/SP/MCH was raised by 10.07 μA compared to the background value in 0.1 M PBS buffer (pH = 7.0) without H_2O_2, owning to the large conjugated structure in polymer chain and reversible electron transfer between PANI (red) and PANI (ox) (L. Bai et al., 2017). When the 2.5 mM H_2O_2 was added into the electrolytic cell (Fig. 3D), the current response was increased to 25.64 μA, which is attributed to the catalysis of H_2O_2 by the PdPt of N-G/PdPt/PANI nanohybrids. For comparison, DPV response of the DNA sensor labelled with N-G/Pd/PANI (Fig. 3B) or N-G/Pt/PANI (Fig. 3C) in 0.1 M PBS buffer (pH7.0) containing 2.5 mM H_2O_2 were also investigated, the current response of 13.61 μA and 18.01 μA were found respectively, which confirmed the effectively catalysis of H_2O_2 by PdPt bimetallic nanoparticles in the N-G/PdPt/PANI nanohybrids with the synergistic effect of the PdPt bimetallic nanoparticles in the N-G/PdPt/PANI nanohybrids (Nantaphol et al., 2017). Accordingly, the N-G/PdPt/PANI/SP/MCH bioconjugate was chosen as a tracer for the sandwich-type DNA biosensor to obtain a superior signal amplification for the following experiments.

3.4. Optimisation of the DNA biosensor preparation conditions

To achieve an optimal performance of the DNA biosensor, some experimental conditions were systematically investigated, including the volume of C_{60}/PAMAM/Au nanomaterial solution, immobilisation time of capture probes, hybridisation time and concentration of H_2O_2. This is shown in Fig. S5, and a detailed description can be found in Supplementary information (S2.4)

3.5. Performance of the DNA biosensor

3.5.1. Analytical performance of the electrochemical DNA biosensor

To evaluate the performance of the electrochemical DNA biosensor, it was employed to detect a standard solution of target DNA at different concentrations under optimal conditions. As shown in Fig. 4A, the DPV responses of the DNA biosensor increased with an increasing concentration of the target DNA. Furthermore, the calibration plot for the quantitative detection of the target DNA is illustrated in Fig. 4B. The peak current change is proportional to the logarithmic value of the target DNA concentrations over approximately six orders of magnitude, ranging from 10 fM to 10 nM with a square of the linear correlation coefficient of 0.99778. The regression equation is Y = 38.48988 + 6.71998 * X with the detection limit of the system is 3.33 fM (signal to noise ratio of 3), indicating that using N-G/PdPt/PANI nanohybrids as the redox probe and catalyst could efficiently enhance the electrochemical response signals and improve the sensitivity of the DNA biosensor. Table S1 gives the associated performance parameters (e.g., responsive strategy, detection limit and linear range) of the current methods for SNP detection. Compared to the other methods for the detection of SNP, the proposed biosensor with N-G/PdPt/PANI nanohybrids for signal generation and amplification shows a wider linear range and lower detection limit, indicating that it may be superior in the trace analysis and rapid and sensitive detection of SNP.

3.5.2. Specificity, reproducibility and stability of the DNA biosensor

To investigate the specificity of the constructed biosensor, interfering substances including single-base-mismatched oligonucleotide (SBM, 1 nM), double-base mismatched DNA (DBM, 1 nM), three-base mismatched DNA (TBM, 1 nM), non-complementary DNA (NC, 1 nM) and the mixtures of these mentioned above with the target DNA (10 pM) were analysed under the same optimised conditions. As shown

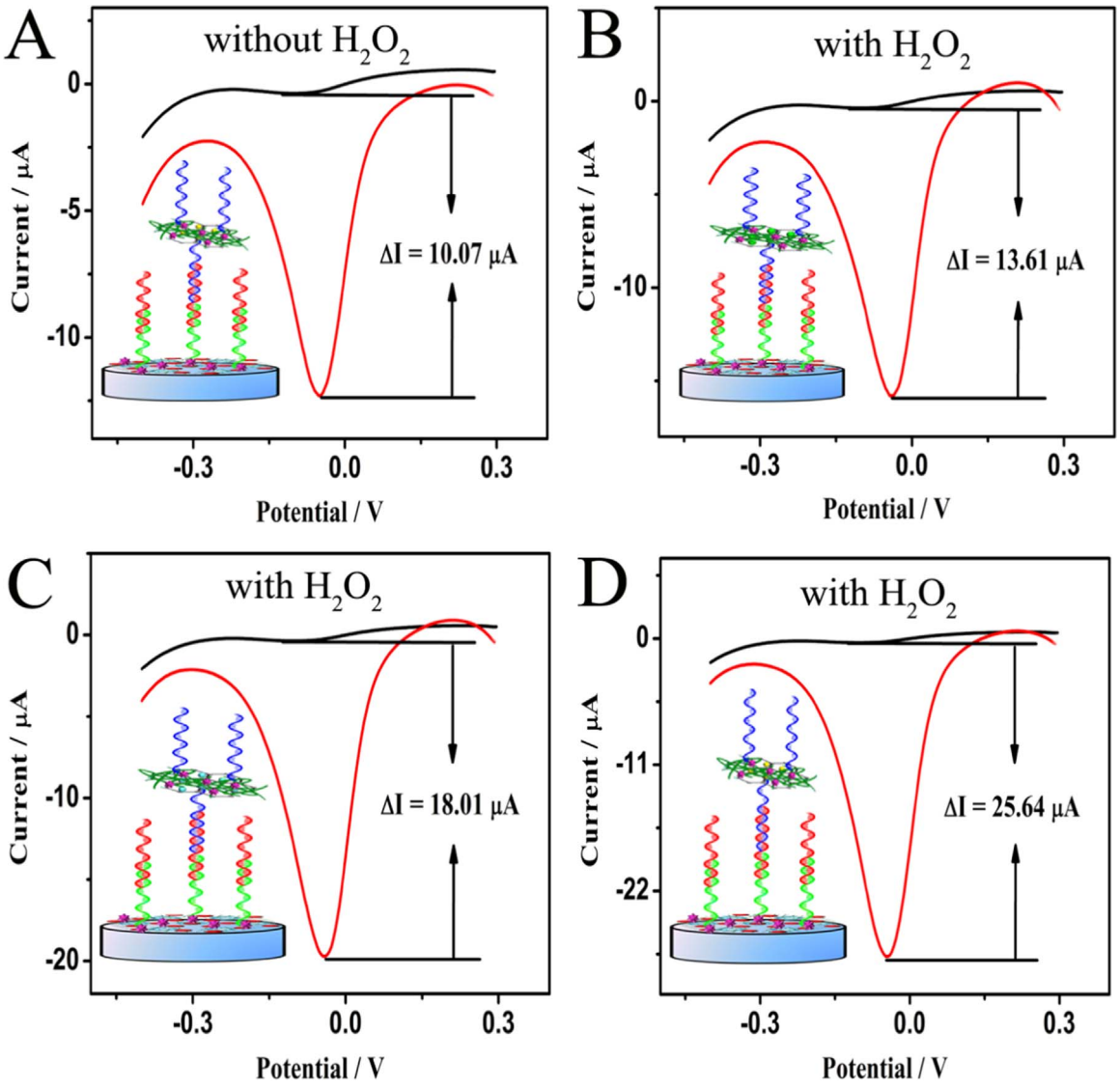

Fig. 3. (A) DPV in the DNA biosensor incubation with N-G/PdPt/PANI/SP/MCH in 0.1 M PBS buffer (pH 7.0) and DPV in the DNA biosensor incubation with different SP bioconjugates: (B) N-G/Pd/PANI/SP/MCH, (C) N-G/Pt/PANI/SP/MCH and (D) N-G/PdPt/PANI/SP/MCH in 0.1 M PBS buffer (pH 7.0) with 2.5 mM H_2O_2.

in Fig. 4C, no apparent changes in the current response of these non-specific interferents were displayed compare to that of the blank test, while a dramatic increase in the current response was shown in the presence of the target DNA (10 pM), and the mixtures exhibited almost identical peak current changes to those of the target DNA. These results indicate that the proposed biosensor exhibits a satisfactory specificity for the detection of the target DNA.

The reproducibility of the DNA biosensor was estimated by using DPV of five DNA biosensors of one-batch and five-batch, which were prepared by incubating 10 pM target DNA under the optimal conditions. As shown in Fig. 4D, the current change showed 0.9585% of the relative standard deviation (RSD) for the intra-batch measurement and 1.9966% of RSD for the inter-batch measurement, indicating high precision and satisfactory reproducibility for the developed DNA biosensor.

Furthermore, the stability of the DNA biosensor was evaluated by long-term storage. The DNA biosensor was stored at 4 °C before use. The DNA biosensor remained bioactive after the first 7 d of storage and the current response showed no obvious change. After 28 d of storage, the final current change was 92.15% of the initial current response (Fig. S6), which suggested that the proposed DNA biosensor exhibits an acceptable stability.

3.5.3. Application for the analysis of spiked human serum samples

To assess the analytical reliability and application of the proposed DNA biosensor to real sample, recovery experiments were performed by standard addition method in spiked serum samples (obtained from the First Affiliated Hospital of Chongqing Medical University, China). As observed in Table 1, the recovery and RSD ranged from 95.97% to 106.01% and from 2.65% to 2.07%, respectively, which demonstrated that the proposed DNA sensor may be have the potential application to construct detection platforms for rs1801177 in LPL gene in clinic.

4. Conclusions

In summary, this is the first report on the use of C_{60}/PAMAM/Au nanocomposites as modified composite film and the novel N-G/PdPt/PANI nanohybrids were synthesised for the detection of SNP in LPL gene electrochemical DNA biosensor. C_{60}/PAMAM/Au nanocomposites with large surface areas were used to immobilise a significant number of CPs. Furthermore, the N-G/PdPt/PANI nanohybrids showed excellent conductivity, catalytic activity, abundant active groups and efficient redox, allowing them be used as the nanocarrier for the signal DNA biosensor and redox probe, increasing the amount of immobilised biomolecules as nanocarriers and efficiently avoiding the leakage of

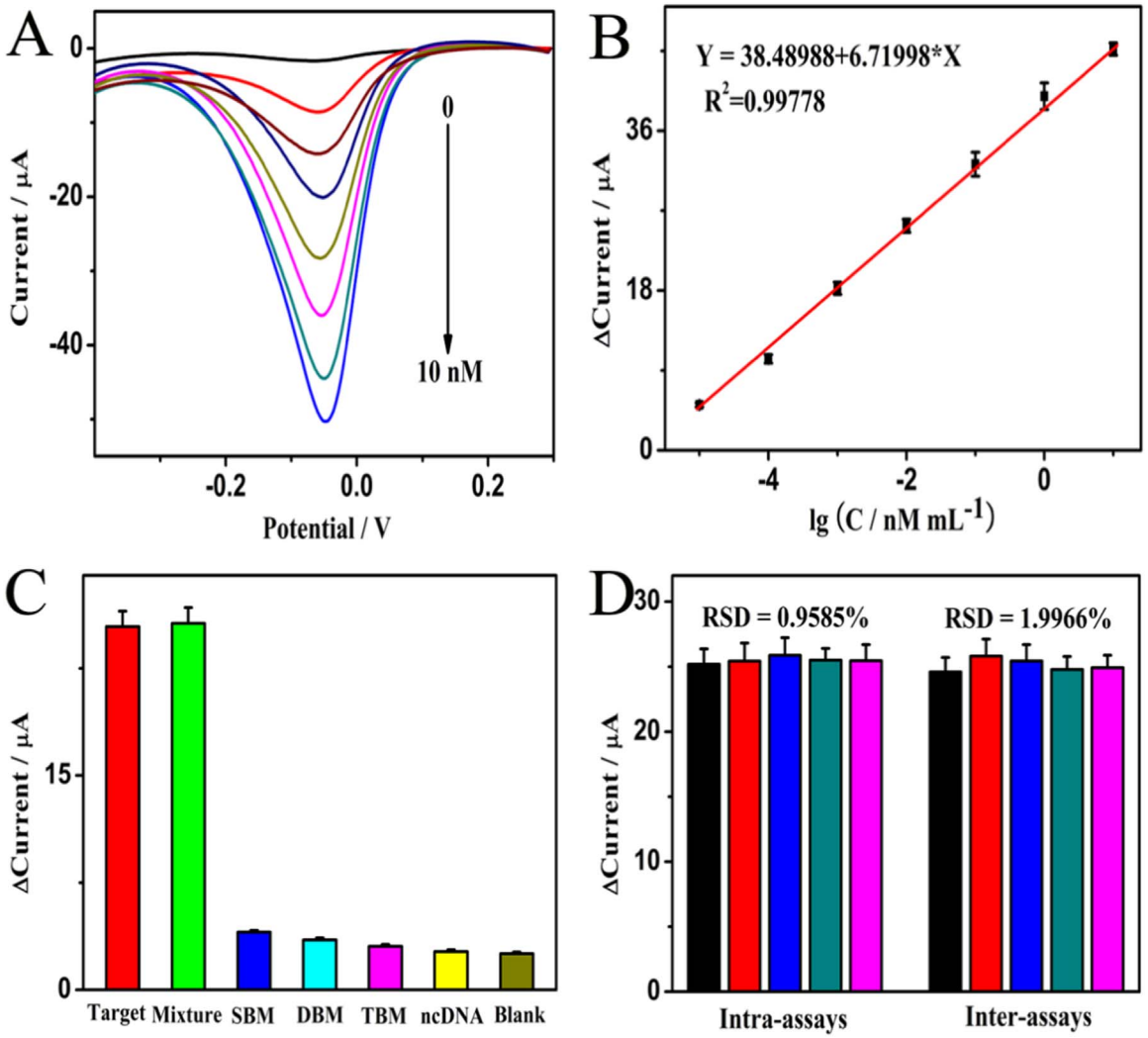

Fig. 4. (A) DPV responses of the proposed DNA biosensor after incubation with different concentrations (10 fM, 100 fM, 1 pM, 10 pM, 100 pM, 1 nM, 10 nM) of target DNA in 0.1 M PBS buffer (pH 7.0) containing 2.5 mM H_2O_2. (B) The calibration curves of DPV peak current change versus the logarithm of target DNA concentration. (C) Specificity of the DNA biosensor toward: blank; non-complementary DNA (ncDNA, 1 nM), three-base mismatched DNA (TBM, 1 nM), double-base mismatched DNA (DBM, 1 nM), single-base mismatched DNA (SBM, 1 nM), mixture of these mentioned above with target DNA (10 pM) and target DNA (10 pM). (D) Reproducibility of the proposed DNA biosensor. The error bars represent the standard deviations of three parallel determination results.

Table 1
Determination of added target DNA in spiked human serum with the proposed DNA biosensor (n = 3).

Serum samples	$C_{analyte}$	Added	Found[a]	Recovery (%)	RSD (%)
Serum-1	NT	100 fM	106.01 fM	106.01	2.07
Serrum-2	NT	10 pM	9.77 pM	97.7	2.7
Serum-3	NT	1 nM	0.9597 nM	95.97	2.65

Samples (1–3) are from healthy people; "NT" indicates not detectable.
[a] The values shown here are averaged from three measurements.

redox molecules. Additionally, nanomaterials themselves act as the redox probe without the additional modification of an electroactive substance and catalyst, which could simplify the operation steps and shorten the analysis time. With the signal amplification through catalysis of H_2O_2 by N-G/PdPt/PANI nanohybrids, the detection signal of the nanohybrids could be significantly enhanced, lead to further improvement in the sensitivity. Moreover, the proposed electrochemical DNA biosensor can be successfully used for the SNP in LPL gene detection in human serum with the advantages including simplicity, rapidity and cost-effectiveness. Therefore, this offers an ideal technology platform for the accurate and rapid identification of SNP in LPL gene in clinic.

Acknowledgment

We are grateful for the financial support from the National Nature Science Foundation of China (No. 81370403), Chongqing foundation and advanced research project (No. CSTC2015jcyjBX0053), Chongqing precision medical key technology research and development and demonstration projects (cstc2016shms-ztzx0042), Chongqing medical university scientific research cultivating fund (No. 201414) and outstanding graduate student cultivation program of Chongqing Medical University (BJRC201724).

Appendix A. Supplementary material

Supplementary data associated with this article can be found in the online version at http://dx.doi.org/10.1016/j.bios.2017.11.054.

References

Adams, B.D., Ostrom, C.K., Chen, A., 2011. J. Electrochem. Soc. 158, B434–B439.
Afreen, S., Kokubo, K., Muthoosamy, K., Manickam, S., 2017. Rsc Adv. 7, 31930–31939.

Afreen, S., Muthoosamy, K., Manickam, S., Hashim, U., 2015. Biosens. Bioelectron. 63, 354–364.
Astruc, D., Boisselier, E., Ornelas, C., 2010. Chem. Rev. 110, 1857–1959.
Bai, L., Chen, Y., Bai, Y., Chen, Y., Zhou, J., Huang, A., 2017a. Biomaterials 133, 11–19.
Bai, R.G., Ninan, N., Muthoosamy, K., Manickam, S., 2017b. Prog. Mater. Sci. 91, 24–69.
Chen, M., Hou, C., Huo, D., Jing, B., Fa, H., Shen, C., 2016. Biosens. Bioelectron. 85, 684–691.
Chen, T., Qiu, J., Zhu, K., Li, J., 2015. J. Mater. Sci.: Mater. Electron. 26, 3730–3738.
Chen, Y., Li, Y., Yang, Y., Wu, F., Cao, J., Bai, L., 2017. Microchim. Acta 184, 1801–1808.
Dhand, C., Das, M., Datta, M., Malhotra, B.D., 2011. Biosens. Bioelectron. 26, 2811–2821.
Ding, S., Huang, H., Xu, Y., Zhu, H., Zhong, C., 2017. BioMed. Res. Int. 8, 1–6.
Geetha, B.R., Muthoosamy, K., Zhou, M., Ashokkumar, M., Huang, N.M., Manickam, S., 2017. Biosens. Bioelectron. 87, 622–629.
Geng, D., Yang, S., Zhang, Y., Yang, J., Liu, J., Li, R., Sham, T.K., Sun, X., Ye, S., Knights, S., 2011. Appl. Surf. Sci. 257, 9193–9198.
Ghadimi, H., Nasiritabrizi, B., Nia, P.M., Wan, J.B., Tehrani, R.M.A., Lorestani, F., 2015. Rsc Adv. 5, 99555–99565.
Han, J., Zhuo, Y., Chai, Y., Yuan, R., Zhang, W., Zhu, Q., 2012. Anal. Chim. Acta 746, 70–76.
Huang, J., Tian, J., Zhao, Y., Zhao, S., 2015. Sens. Actuators B-Chem. 206, 570–576.
Izar, M.C., Helfenstein, T., Ihara, S.S., Relvas, W.G., Santos, A.O., Fischer, S.C., Pinto, L.E., Lopes, I.E., Pomaro, D.R., Fonseca, M.I., 2009. Atherosclerosis 204, 165–170.
Jian-Min, Wang, En-Fang, Hai-Long, Wang, Wen-Long, Jing, Le-Le, Zhao, Zhen-Lin, 2017. Chin. Chem. Lett. 2, 383–387.
Jiang, D., Liu, Q., Wang, K., Qian, J., Dong, X., Yang, Z., Du, X., Qiu, B., 2014. Biosens. Bioelectron. 54, 273–278.
Jukema, J.W., Van Boven, A.J., Zwinderman, A.H., Reiber, J.H., Bruschke, A.V., Henneman, J., Molhoek, G., Bruin, T., Jansen, H., Gagne, E., 1996. Circulation 94, 1913–1918.
Junyent, M., Tucker, K.L., Shen, J., Lee, Y.-C., Smith, C.E., Mattei, J., Lai, C.-Q., Parnell, L.D., Ordovas, J.M., 2010. Nutr. Metab. Cardiovasc. Dis. 20, 157–164.
Lai, G., Yan, F., Ju, H., 2009. Anal. Chem. 81, 9730–9736.
Li, M., Wang, P., Li, F., Chu, Q., Li, Y., Dong, Y., 2017a. Biosens. Bioelectron. 87, 752–759.
Li, Y., Zhang, Y., Li, F., Feng, J., Li, M., Lei, C., Dong, Y., 2017b. Biosens. Bioelectron. 92, 33–39.
Liu, S., Xing, X., Yu, J., Lian, W., Li, J., Cui, M., Huang, J., 2012. Biosens. Bioelectron. 36, 186–191.
Liu, X., Ma, D., Tang, H., Tan, L., Xie, Q., Zhang, Y., Ma, M., Yao, S., 2014. ACS Appl. Mater. Inter. 6, 8173–8183.
Ma, R.T., Zhao, H.T., Zhang, G., 2010. Mater. Res. Bull. 45, 1064–1068.
Nantaphol, S., Watanabe, T., Nomura, N., Siangproh, W., Chailapakul, O., Einaga, Y., 2017. Biosens. Bioelectron. 98, 76–82.
Pichler, M., Balic, M., Stadelmeyer, E., Ausch, C., Wild, M., Guelly, C., Bauernhofer, T., Samonigg, H., Hoefler, G., Dandachi, N., 2009. J. Mol. Diagn. 11, 140–147.
Prasad, B.B., Singh, R., Kumar, A., 2017. Biosens. Bioelectron. 94, 115–123.
Pu, L.-M., Long, H.-T., Zhang, Y., Bai, Y., Dong, W.-K., 2017. Polyhedron 128, 57–67.
Rebhi, L., Kchok, K., Omezzine, A., Kacem, S., Rejeb, J., HadjMbarek, I.B., Belkahla, R., Boumaiza, I., Moussa, A., Rejeb, N.B., 2012. Mol. Biol. Rep. 39, 9893–9901.
Ruiyi, L., Ling, L., Hongxia, B., Zaijun, L., 2016. Biosens. Bioelectron. 79, 457–466.
Shahid, S.U., Shabana, N., Cooper, J.A., Rehman, A., Humphries, S.E., 2017. Lipids Health Dis. 16, 24–30.
Sivakumar, M., Gedanken, A., 2005. Synth. Met. 148, 301–306.
Tapiavieyra, J.V., Delgadocoello, B., Masoliva, J., 2017. Arch. Med. Res. 48, 12–26.
Thanh, T.D., Balamurugan, J., Lee, S.H., Kim, N.H., Lee, J.H., 2016. Biosens. Bioelectron. 81, 259–267.
Wang, C.Z., Lin, J., Qian, J., Shao, R., Xue, D., Qian, W., Xiao, G.F., Deng, Z.Q., Yang, J., Li, Y., 2013a. Clin. Biochem. 46, 385–387.
Wang, P., Tan, K.L., Kang, E.T., Neoh, K.G., 2002. J. Membr. Sci. 195, 103–114.
Wang, Z.G., Zhan, P., Ding, B., 2013b. Acs Nano 7, 1591–1598.
Xu, Y., Dai, L., Chen, J., Gal, J.Y., Wu, H., 2007. Eur. Polym. J. 43, 2072–2079.
Yang, G., Li, L., Rana, R.K., Zhu, J.J., 2013. Carbon 61, 357–366.
Yao, G.H., Liang, R.P., Huang, C.F., Wang, Y., Qiu, J.D., 2013. Eur. Polym. J. 85, 11944–11951.
Yin, J., Zhao, X., Xia, X., Xiang, L., Qiao, Y., 2008. Polymer 49, 4413–4419.
Zan, X., Fang, Z., Wu, J., Xiao, F., Huo, F., Duan, H., 2013. Biosens. Bioelectron. 49, 71–78.
Zhang, H., Lu, Q., Zuo, F., Yuan, R., Chen, S., 2017. Sens. Actuators, B 241, 887–894.
Zhang, J., Jiang, J., Li, H., Zhao, X.S., 2011. Energy Environ. Sci. 4, 4009–4015.
Zhang, R., Zhu, Z., Zhu, H., Tu, N., Yao, F., Xia, K., Liang, D., Liu, C., 2005. Nucleic Acids Res. 33, W489–W492.
Zheng, Z., Du, Y., Feng, Q., Wang, Z., Wang, C., 2012. J. Mol. Catal. A Chem. 353–354, 80–86.
Zhong, X., Yuan, R., Chai, Y., 2012. Chem. Commun. 48, 597–599.